Inorganic Chemistry
Article

Inorg. Chem. **2010**, *49*, 1039–1045 **1039**
DOI: 10.1021/ic901916q

Gas-Phase Structures of Iron Trihalides: A Computational Study of all Iron Trihalides and an Electron Diffraction Study of Iron Trichloride

Zoltán Varga, Mária Kolonits, and Magdolna Hargittai*

Materials Structure and Modeling Research Group of the Hungarian Academy of Sciences, Budapest University of Technology and Economics, P.O. Box 91, 1521 Budapest, Hungary

Received September 29, 2009

The molecular structures of the monomers and dimers of all iron trihalides, FeF_3, $FeCl_3$, $FeBr_3$, and FeI_3, were determined by computations, and the structure of iron trichloride monomers and dimers was determined also by gas-phase electron diffraction. The thermal-average bond length, r_g, of $FeCl_3$ is 2.136(5) Å, and the estimated equilibrium bond length from experiment, 2.122(6) Å, is in excellent agreement with the computed value. Vibrational and thermodynamic properties have also been calculated for all species. The stability of iron trihalides decreases toward the iodide; neither the bromide nor the iodide can be evaporated without decomposition. The structures of isomers of trimers and tetramers for iron trichloride have also been calculated. The connection between the gas-phase and crystal-phase structures and the exceptional stability of the dimer is discussed.

Introduction

Among the halides of iron, oxidation states +2 and +3 are the most common, with the trihalides becoming less and less stable than the dihalides with increasing halogen size. In this paper, the structural and thermodynamic properties of all iron trihalides are discussed based on high-level computations, and in the case of $FeCl_3$, in addition, on high-temperature gas-phase electron diffraction (ED). From the point of view of applications, iron trichloride is the most important in the group; it is used extensively for wastewater treatment, purification of drinking water, and in catalytic processes. Iron trichloride was the first inorganic contrast agent used in a human in magnetic resonance imaging; it was administered orally for gastrointestinal tract imaging.[1] $FeBr_3$ is a Lewis acid, and it is applied as catalyst in the halogenation of aromatic compounds.

FeF_3 evaporates at high temperature as a monomeric molecule, and its structure has been determined by gas-phase ED.[2−4] In contrast, iron trichloride evaporates at relatively low temperature as a dimer as witnessed by mass spectrometric[5,6] and ED[7] studies. It is only at higher temperatures that the iron trichloride monomers appear in the vapor; and upon further heating, they decompose into the dichloride.[8] Iron tribromide cannot be sublimed unless a larger than 1 atm pressure of bromine is applied.[9] Ferric iodide cannot be evaporated without decomposition; it was isolated in the solid state for the first time just in 1988.[10] The crystals of FeF_3 have a rhombohedral structure that is intermediate between hexagonal closest packing and cubic closest packing,[11−13] while those of iron trichloride[14−16] and tribromide[17] are hexagonal layer structures; the iron coordination is octahedral in all of them. Dimeric units are present in the melts of iron

*To whom correspondence should be addressed. E-mail: hargittaim@mail.bme.hu.

(1) Young, I. R.; Clarke, G. J.; Bailes, D. R.; Pennock, J. M.; Doyle, F. H.; Bydder, G. M. *J. Comput. Tomogr.* **1981**, *5*, 543–547.
(2) Hargittai, M.; Kolonits, M.; Tremmel, J.; Fourquet, J.-L.; Ferey, G. *Struct. Chem.* **1990**, *1*, 75–78.
(3) Girichev, G. V.; Kostyushin, D. A.; Petrova, V. N.; Shlykov, S. A. *J. Struct. Chem.* **1991**, *32*, 503–507.
(4) Hargittai, M. *J. Chem. Phys.* **2005**, *123*, 196101.
(5) Wilson, L. E.; Gregory, N. W. *J. Phys. Chem.* **1958**, *62*, 433–437.
(6) Hammer, R. R.; Gregory, N. W. *J. Phys. Chem.* **1962**, *66*, 1705–1707.
(7) Hargittai, M.; Tremmel, J.; Hargittai, I. *J. Chem. Soc., Dalton Trans.* **1980**, 87–89.
(8) Greenwood, N. N.; Earnshaw, A. *Chemistry of the Elements*; Pergamon Press: Elmsford, NY, 1984.
(9) Gregory, N. W.; Thackey, B. A. *J. Am. Chem. Soc.* **1950**, *72*, 3176–3178.
(10) Yoon, K. B.; Kochi, J. K. *Z. Anorg. Allg. Chem.* **1988**, *561*, 174–184.
(11) Hepworth, M. A.; Jack, K. H.; Peacock, R. D.; Westland, G. J. *Acta Crystallogr.* **1957**, *10*, 63–69.
(12) Leblanc, M.; Pannetier, J.; Ferey, G.; Depape, R. *Rev. Chim. Min.* **1985**, *22*, 107–114.
(13) Wells, A. F. *Structural Inorganic Chemistry*, 4th ed.; Clarendon Press: Oxford, 1975.
(14) Wooster, N. *Z. Kristallogr.* **1932**, *83*, 35–41.
(15) Geierberger, K. *Z. Anorg. Chem.* **1949**, *258*, 361–363.
(16) Hashimoto, S.; Forster, K.; Moss, S. C. *J. Appl. Crystallogr.* **1989**, *22*, 173–180.
(17) Gregory, N. W. *J. Am. Chem. Soc.* **1951**, *73*, 472–473.
(18) Price, D. L.; Saboungi, M. L.; Badyal, Y. S.; Wang, J.; Moss, S. C.; Leheny, R. L. *Phys. Rev. B: Condens. Matter* **1998**, *57*, 10496–10503.
(19) Papatheodorou, G. N.; Voyiatzis, G. A. *Chem. Phys. Lett.* **1999**, *303*, 151–156.
(20) Sitze, M. S.; Schreiter, E. R.; Patterson, E. V.; Freeman, R. G. *Inorg. Chem.* **2001**, *40*, 2298–2304.
(21) Akdeniz, Z.; Tosi, M. P. *Z. Naturforsch., A: Phys. Sci.* **1998**, *53*, 960–962.

Published on Web 01/05/2010

trichloride, according to neutron diffraction,[18] Raman spectroscopy,[19,20] and computer simulation.[21−23]

Prior computational studies of iron trihalides include the recent studies of iron trifluoride[24,25] and the earlier calculations of iron trichloride monomer[26] and the iron trichloride dimer.[27] We are not aware of a complete computational study of the whole iron trihalide series. Experimental vibrational spectroscopic studies have appeared on iron trifluoride[28,29] by matrix isolation infrared (IR) spectroscopy and on iron trichloride by gas-phase IR[30] and Raman,[31,32] matrix IR[33] and Raman[34] spectroscopy, see also ref 35.

We did an ED study of iron trichloride 30 years ago at a nozzle temperature of about 460 K at which the vapor consisted of only dimeric molecules.[7] In the present work, we report the high-temperature ED study of iron trichloride with the aim of determining the structure of its monomer. Since at the time of the earlier study the possible anharmonicity of the stretching vibrations was not considered in the analysis, we reanalyzed the earlier data set for the dimer as well. We have also computed the structure of all four iron trihalide monomers and dimers. Vibrational frequencies for all species were also calculated and NBO analyses were carried out to see the occupation of the 3d orbitals and the extent and effect of covalent bonding.

The primary purpose of this investigation was, beyond providing reliable information on the individual structures, to see whether, and what kind of, trends could be observed in the structural variations in this important group of substances.

Computational Details

Most of the computations were carried out using the unrestricted mPW1PW91 DFT method,[36] that appears to provide geometrical data for metal halides in good agreement with experiments. All computations were performed using the Gaussian03 program package.[37] For checking the possibility of antiferromagnetic coupling in the dimers, MRCI calculations were also carried out for Fe_2Cl_6; for these the MOLPRO program was used.[38]

The iron atom was described by a relativistic effective core potential[39] (MDF ECP, describing 10 electrons) and its associated valence basis set (8s7p6d2f1g)/[6s5p3d2f1g].[39,40] The two smaller halogen atoms were described by Dunning type all-electron cc-pVQZ (F^{41} and Cl^{42}) basis sets and the two larger ones with a relativistic MDF-ECP and the corresponding cc-pVQZ-PP (Br^{43} and recalculated I^{44}) basis sets. These provided balanced basis sets for the one used for iron.

Beside the DFT method, we also carried out MP2 level calculations[45] for $FeCl_3$, Fe_2Cl_6, and Fe_2I_6. For iron trichloride, comparison with the experimental results and the ones available in the literature warranted these calculations. For the iron triiodide dimer, the DFT method yielded a C_{2v}-symmetry puckered structure; hence, we found it necessary to calculate the structure with another method as well. In the MP2 calculations we used the ReadWindow (RW) suboption with 20,0 and 39,0 orders for iron trichloride and a 63,0 order for iron triiodide, respectively, to ensure that only the valence shell is taken into consideration in the calculation.

The potential energy surface for the ring puckering vibration of Fe_2Cl_6 was also calculated to aid the dynamic ED analysis of this molecule (vide infra). For this, the structure of the dimer was calculated in the puckering-angle range between 0 and 40 degrees at 5 degree intervals, and their contributions to the scattering were included according to their Boltzmann-distribution at 460 and 900 K, respectively.

For the iron trichloride dimers both high-spin ($^1B_{1g}$) and low-spin ($^1B_{1g}$) electronic states were calculated at the DFT (mPW1PW91) and the MRCI levels of theory, resulting in rather different energies (vide infra). To find connection between the gas-phase and crystal-phase structures of iron trihalides, we also calculated the structures of some iron trichloride trimers and tetramers. Their Cartesian coordinates are given in Supporting Information, Table S1. The stability of all structures was verified by frequency calculations (mPW1PW91 level); the frequencies of the monomers and dimers of all trihalides are given in Supporting Information, Tables S2 and S3, respectively, together with the available experimental frequencies from the literature. The agreement between experiment and computation is satisfactory, with differences not larger than between the sometimes rather

(22) Akdeniz, Z.; Pastore, G.; Tosi, M. P. *Phys. Chem. Liq.* **1997**, *35*, 93–104.
(23) Goat, E.; Ruberto, R.; Pastore, G.; Akdeniz, Z.; Tosi, M. P. *Phys. Chem. Liq.* **2007**, *45*, 487–501.
(24) Solomonik, V. G.; Stanton, J. F.; Boggs, J. E. *J. Chem. Phys.* **2005**, *122*, 094322.
(25) Solomonik, V. G.; Stanton, J. F.; Boggs, J. E. *J. Chem. Phys.* **2008**, *128*, 244104.
(26) Bach, R. D.; Shobe, D. S.; Schlegel, H. B.; Nagel, C. J. *J. Phys. Chem.* **1996**, *100*, 8770–8776.
(27) Scholz, G.; Curtiss, L. A. *THEOCHEM* **2000**, *507*, 245–251.
(28) Predtechenskii, Y. B.; Schcherba, L. D. *Vibrational Spectra Application in Inorganic and Coordination Chemistry, Proceeding of the 12th All-Union Symposium*, Minks, USSR **1989**.
(29) Osin, S. B.; Davliatshin, D. I.; Ogden, J. S. *J. Fluorine Chem.* **1996**, *76*, 187–192.
(30) Wilmshurst, J. K. *J. Mol. Spectrosc.* **1961**, *5*, 343–354.
(31) Papatheodorou, G. N. In *Characterization of High-Temperature Vapors and Gases*; Hastie, J. W., Ed.; National Bureau of Standards: Gaithersburg, MD, 1978; p 647.
(32) Nalbandian, L.; Papatheodorou, G. N. *High Temp. Sci.* **1989**, *28*, 49–65.
(33) Frey, R. A.; Werder, R. D.; Günthard, H. H. *J. Mol. Spectrosc.* **1970**, *35*, 260–283.
(34) Givan, A.; Lowenschuss, A. J. *J. Raman Spectrosc.* **1977**, *6*, 84–88.
(35) Hargittai, M. *Chem. Rev.* **2000**, *100*, 2233–2301.
(36) Adamo, C.; Barone, V. *J. Chem. Phys.* **1998**, *108*, 664–675.
(37) Frisch, M. J.; Trucks, G. W.; Schlegel, H. B.; Scuseria, G. E.; Robb, M. A.; Cheeseman, J. R.; Montgomery Jr., J. A.; Vreven, T.; Kudin, K. N.; Burant, J. C.; Millam, J. M.; Iyengar, S. S.; Tomasi, J.; Barone, V.; Mennucci, B.; Cossi, M.; Scalmani, G.; Rega, N.; Petersson, G. A.; Nakatsuji, H.; Hada, M.; Ehara, M.; Toyota, K.; Fukuda, R.; Hasegawa, J.; Ishida, M.; Nakajima, T.; Honda, Y.; Kitao, O.; Nakai, H.; Klene, M.; Li, X.; Knox, J. E.; Hratchian, H. P.; Cross, J. B.; Bakken, V.; Adamo, C.; Jaramillo, J.; Gomperts, R.; Stratmann, R. E.; Yazyev, O.; Austin, A. J.; Cammi, R.; Pomelli, C.; Ochterski, J. W.; Ayala, P. Y.; Morokuma, K.; Voth, G. A.; Salvador, P.; Dannenberg, J. J.; Zakrzewski, V. G.; Dapprich, S.; Daniels, A. D.; Strain, M. C.; Farkas, O.; Malick, D. K.; Rabuck, A. D.; Raghavachari, K.; Foresman, J. B.; Ortiz, J. V.; Cui, Q.; Baboul, A. G.; Clifford, S.; Cioslowski, J.; Stefanov, B. B.; Liu, G.; Liashenko, A.; Piskorz, P.; Komaromi, I.; Martin, R. L.; Fox, D. J.; Keith, T.; Al-Laham, M. A.; Peng, C. Y.; Nanayakkara, A.; Challacombe, M.; Gill, P. M. W.; Johnson, B.; Chen, W.; Wong, M. W.; Gonzalez, C.; Pople, J. A. *Gaussian 03*; Gaussian, Inc.: Wallingford, CT, 2003.
(38) Werner, H.-J.; Knowles, P. J.; Lindh, R.; Manby, F. R.; Schütz, M.; Celani, P.; Korona, T.; Rauhut, G.; Amos, R. D.; Bernhardsson, A.; Berning, A.; Cooper, D. L.; Deegan, M. J. O.; Dobbyn, A. J.; Eckert, F.; Hampel, C.; Hetzer, G.; Lloyd, A. W.; McNicholas, S. J.; Meyer, W.; Mura, M. E.; Nicklass, A.; Palmieri, P.; Pitzer, R.; Schumann, U.; Stoll, H.; Stone, A. J.; Tarroni, R.; Thorsteinsson, T. *MOLPRO*; 2006. http://www.molpro.net.
(39) Dolg, M.; Wedig, U.; Stoll, H.; Preuss, H. *J. Chem. Phys.* **1987**, *86*, 866–872.
(40) Martin, J. M. L.; Sundermann, A. *J. Chem. Phys.* **2001**, *114*, 3408–3420.
(41) Dunning, T. H. *J. Chem. Phys.* **1989**, *90*, 1007–1023.
(42) Woon, D. E.; Dunning, T. H. *J. Chem. Phys.* **1993**, *98*, 1358–1371.
(43) Peterson, K. A.; Figgen, D.; Goll, E.; Stoll, H.; Dolg, M. *J. Chem. Phys.* **2003**, *119*, 11113–11123.
(44) Peterson, K. A.; Shepler, B. C.; Figgen, D.; Stoll, H. *J. Phys. Chem. A* **2006**, *110*, 13877–13883.
(45) Møller, C.; Plesset, M. S. *Phys. Rev.* **1934**, *46*, 618–622.

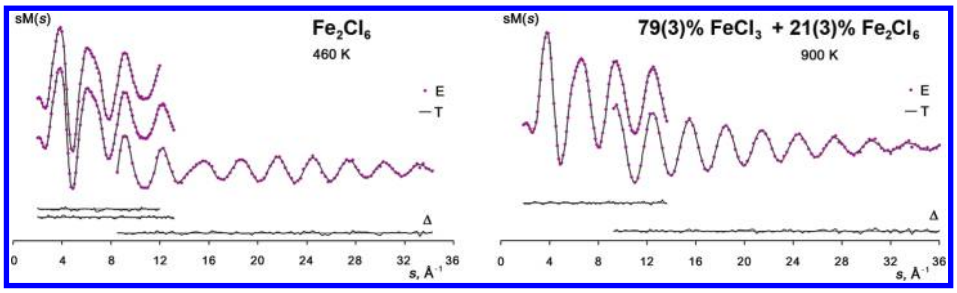

Figure 1. ED molecular intensities (E, experimental; T, theoretical) and their differences (Δ) for iron trichloride at the two experimental temperatures.

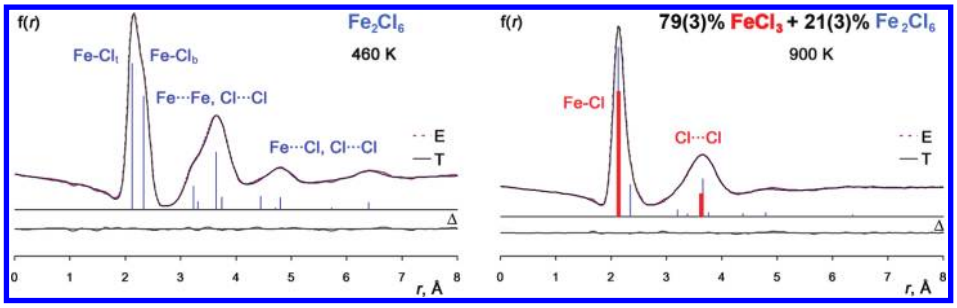

Figure 2. Radial distributions (E, experimental; T, theoretical) and their differences (Δ) for iron trichloride at the two experimental temperatures. The contribution of different distances is indicated by vertical bars.

scattered experimental values. Natural Bond Orbital (NBO)[46] and Wiberg bond index analyses[47] were carried out for all molecules. Some thermodynamic parameters were also calculated.

ED Experiment and Structure Analysis

The ED patterns of the $FeCl_3$ sample were recorded with the combined ED−quadrupole mass-spectrometric experiment developed in the Budapest laboratory,[48,49] with a modified EG-100A apparatus and a double-oven nozzle system.[50] The acceleration voltage was 60 kV. The sample of iron-trichloride was a 99.99+% purity Aldrich product. The nozzle material was stainless steel covered with platinum foil, and the nozzle system was passivated with chlorine gas before the experiment. The nozzle temperature was 900(50) K. The ΔG values of the dimerization of $FeCl_3$ in Supporting Information, Table S4 indicate that at 900 K the dissociation is favored. Six photographic plates were used in the analysis at both camera ranges. The data intervals were 1.875−13.625 Å^{-1} (with 0.125 Å^{-1} steps) and 9.25−36.00 Å^{-1} (with 0.25 Å^{-1} steps) at 50 and 19 cm camera ranges, respectively. The details of the low-temperature experiment are given in ref 7. Experimental ED molecular intensities are available in Supporting Information, Table S5. The molecular intensities for both low- and high-temperature experiments are given in Figure 1 with the corresponding radial distributions in Figure 2. Normal coordinate analyses were performed using the program ASYM20[51] for both monomeric and dimeric iron trichloride. Vibrational amplitudes were calculated from the computed harmonic vibrational frequencies and force fields and were used as starting parameters in the ED analysis. For the monomer molecule, the amplitudes were also calculated from the experimental vibrational frequencies;[31] there was good agreement with the computed ones.

First we reanalyzed our earlier low-temperature (460 K) ED data.[7] We wanted to see how the possible anharmonicity of the stretching vibrations, not accounted for in the earlier study, influences the results for the bond lengths. In this analysis we used the new electron scattering factors (the same as for the new high-temperature experiment).[52] We also wanted to aid the structure analysis of the new high-temperature experimental data and have a consistent analysis scheme for the two sets of data so that the temperature effect on the structure of the dimer could be observed. To avoid high correlation among the parameters, a dynamic analysis was performed for the dimer, based on the computed puckering potential of the four-member ring of the dimer (see Computational Section). The geometries of the differently puckered models were calculated based on the computed parameter differences relative to the D_{2h}-symmetry model. The independent parameters refined during the structure analysis were the following, all referring to the D_{2h}-symmetry molecule: the average of the terminal and bridging bond lengths, their difference, and the terminal and bridging bond angle. At the beginning of the structure analysis the average and the difference of bond lengths were refined one after the other. However, at later stages, all independent parameters were refined simultaneously. The vibrational amplitudes of all distances were refined in groups, and the asymmetry parameters of the bond lengths were also refined together.

In the analysis of the high-temperature experimental data, the presence of dimeric molecules had to be taken into account beside the possible presence of the decomposition product, $FeCl_2$. The latter could be ruled out during the refinement (in fact, the radial distribution curve exhibits no contribution around 4.2 Å, where the Cl···Cl distance of the $FeCl_2$ molecule should appear). The dimers were treated with a dynamic model, similar to the case of the low-temperature experiment, but the distribution of the puckered structures was recalculated for the higher temperature. The initial values

(46) Reed, A. E.; Curtiss, L. A.; Weinhold, F. *Chem. Rev.* **1988**, *88*, 899–926.
(47) Wiberg, K. *Tetrahedron* **1968**, *24*, 1083–1096.
(48) Hargittai, I.; Tremmel, J.; Kolonits, M. *HIS, Hung. Sci. Instrum.* **1980**, *50*, 31–42.
(49) Hargittai, I.; Bohatka, S.; Tremmel, J.; Berecz, I. *HIS, Hung. Sci. Instrum.* **1980**, *50*, 51–56.
(50) Tremmel, J.; Hargittai, I. *J. Phys. E: Sci. Instrum.* **1985**, *18*, 148–150.
(51) Hedberg, L.; Mills, I. M. *J. Mol. Spectrosc.* **1993**, *160*, 117–142.
(52) Ross, A. W.; Fink, M.; Hilderbrandt, R.; Wang, J.; Smith Jr., V. H. In *International Tables for Crystallography Vol. C*; Wilson, A. J. C., Ed.; Kluwer: Dordrecht, 1995; pp 245−338.

Table 1. Computed Bond Lengths of FeX_3 ($^6A_1'$) Monomer Molecules (r_e, in Å)

	this work			literature values
method	MP2	DFT[a]	ED (exp)	for method, see footnote
F		1.741	1.750(4)[b]	1.737[c], 1.745[d]
Cl	2.118	2.122	2.122(6)[e]	2.144[f], 2.139[g], 2.144[h], 2.144[h], 2.105[h]
Br		2.265		
I		2.468		

[a] mPW1PW91/ECP10MDF/cc-pVQZ(-PP). [b] Estimated experimental equilibrium bond length, r_e^M; calculated from the thermal-average parameters from refs 2 and 4. [c] Estimated for CBS limit at CCSD(T) level of theory ref 24. [d] Estimated for CBS-DK limit at CCSD(T) level of theory ref 25. [e] Estimated experimental equilibrium bond length, r_e^M; this work, from the thermal-average bond length, see Table 3. [f] HF/WD95* from ref 27. [g] B3LYP/6-31G* from ref 20. [h] B3LYP, QCISD, and MP2; double-ζ + polarization for each method, respectively, ref 26.

of the dimer vibrational amplitudes were assumed based on their values in the low-temperature experiment, taking into account the temperature increase by adjusting them according to the ratios of the calculated amplitudes for the two different temperatures. The independent parameters refined during the structure analysis were the average of the monomer and the dimer terminal bond lengths, their difference, the difference of the two dimer bond lengths, the monomer Cl···Cl non-bonded distance, the two bond angles of the dimer, and the monomer/dimer ratio. On the basis of our computation, initially the difference of the monomer and the dimer terminal bond lengths was assumed to be zero; at later stages we attempted to refine it but that turned out to be impossible. Therefore, we checked how small changes in this parameter affected the results and took this into account in the estimation of the uncertainties. The two monomer vibrational amplitudes, together with most vibrational amplitudes of the dimer, were refined in groups. The asymmetry parameters of the monomer bond length and the two dimer bond lengths were also refined in a group. During the structure analysis it became clear that the terminal bond angle of the dimer cannot be refined; therefore, we accepted the value of this angle from the low-temperature experiment. By using different values for this bond angle in a rather wide range, we determined the influence of this constraint on the other parameters, and this was taken into account in the error estimation. About one-quarter of all molecules were dimers in the vapor, amounting to a little more than half of the scattering power of the sample. However, its impact on the determination of the monomer geometry was much diminished because most of the dimer contribution soon disappeared beyond the small-angle region in the molecular intensities (see the Supporting Information, Figure S1). A so-called "static analysis" was also performed to see whether the different refinement methods influence the results—they did not.

Computational Results

Monomer. Table 1 presents the computed monomer bond lengths, together with other computational results from the literature and the available experimental data. For FeF_3, two high-level computations are available, in which the complete basis set limit (CBS) was estimated; our DFT calculation falls between the two CCSD(T) values, and their agreement can be considered satisfactory, considering the large difference in the computational level. The estimated experimental equilibrium bond length, 1.750(4) Å is a few thousands of an Å larger than the computed values, but considering the about 1300 K experimental temperature and the approximate character of the estimation, the agreement is good.

For $FeCl_3$, several computational results with varying levels of methods and basis sets are available in the literature with a wide range of computed bond lengths (see Table 1). The MP2 calculation of ref 26 gave a much too short bond. Our MP2 bond is also somewhat short, in accordance with earlier experience with the MP2 method for metal halides.[53−55] The other Fe−Cl bond lengths from the literature are around 2.14 Å, about 0.02 Å larger than our DFT value; possibly because of the lower quality of the basis sets (mostly of double-ζ quality) applied in these studies; apparently, they were not satisfactory for this system.

Table 2. Computed Geometrical Parameters of the Fe_2X_6 ($^{11}B_{1g}$) Dimers (Bond Length, r_e, in Å, Angles in deg)[a]

X	method	Fe−X_t	Fe−X_b	X_t−Fe−X_t	X_b−Fe−X_b	puck
F	DFT	1.735	1.934	119.7	79.5	0.0
Cl	DFT	2.122	2.336	117.3	91.7	0.0
	MP2	2.115	2.327	119.5	91.1	0.0
	Lit.[b]	2.135	2.384	120.0	85.0	0.0
	ED[c]	2.122(6)	2.317(13)			
Br	DFT	2.268	2.484	116.6	94.5	0.0
I	DFT	2.477	2.685	115.4	96.8	15.2
	MP2[d]	2.516	2.875	159.4	91.0	23.0

[a] This work unless indicated otherwise. For details of applied methods, see Computational section. X_t refers to the terminal; X_b to the bridging halogen atoms; puck is the puckering angle of the central four-member ring of the dimer along the $X_b\cdots X_b$ axis. [b] The highest level calculation from ref 27. [c] Estimated experimental equilibrium bond length, r_e^M; from the thermal-average bond length at 900 K, see Table 3. [d] For discussion of this very different structure, see the Discussion.

Dimer. Table 2 displays the computed geometrical parameters of all four iron trihalide dimers (high-spin structures, $^{11}B_{1g}$ electronic state). They all have a structure with two halogen bridges but of different symmetry. In each case, the terminal bond length of the dimer is about the same as that of the monomer; their difference is never larger than 0.01 Å. The difference between the two dimer bond lengths is about 0.2 Å, according to the general experience with such halogen-bridged molecules.[35,56]

The bridging bond angle increases appreciably in going from the fluoride toward the iodide; from about 80° in the trifluoride to about 97° in the triiodide. This is easily explained by the stress within the four-member ring because of the closeness of the gradually larger and larger halogen atoms. For the rather small, about 80° bond angle in Fe_2F_6 repulsion between the iron atoms in the ring might also be responsible. The terminal bond angle decreases, but only slightly, from the fluoride (119.7°) toward the iodide (115.4°), according to our DFT studies. Some peculiarities of the computed Fe_2I_6 structure will be mentioned in the Discussion.

(53) Lanza, G.; Varga, Z.; Kolonits, M.; Hargittai, M. *J. Chem. Phys.* **2008**, *128*, 074301.
(54) Vest, B.; Varga, Z.; Hargittai, M.; Hermann, A.; Schwerdtfeger, P. *Chem.—Eur. J.* **2008**, *14*, 5130–5143.
(55) Groen, C. P.; Varga, Z.; Kolonits, M.; Peterson, K. A.; Hargittai, M. *Inorg. Chem.* **2009**, *48*, 4143–4153.
(56) Hargittai, M. In *Stereochemical Applications of Gas-Phase Electron Diffraction. Part B: Structural Information for Selected Classes of Compounds*; Hargittai, I., Hargittai, M., Eds.; VCH Publishers: New York, 1988; pp 383−454.

Table 3. Geometrical Parameters of $FeCl_3$ and Fe_2Cl_6 from ED[a]

	T = 460K		T = 900K
	earlier analysis[7]	present work	present work
	Monomer		
r_g(Fe−Cl)			2.136(5)
r_e^M(Fe−Cl)			2.122(6)
l(Fe−Cl)			0.068(2)
κ(Fe−Cl) × 10^{-5}			2.0(3)
r_g(Cl···Cl)			3.642(13)
l(Cl···Cl)			0.200(7)
$\angle_a$(Cl−Fe−Cl)[b]			116.6(6)
%(monomer)			79(3)
	Dimer		
r_a⟨Fe−Cl⟩[c]	2.227(4)	2.229(4)	
Δr_a(Fe−Cl_b)−(Fe−Cl_t)[d]	0.199(3)[e]	0.202(3)[e]	0.212(10)
Δr_a(Fe−Cl)$_M$−(Fe−Cl_t)[f]			[0.000]
r_g(Fe−Cl_t)	2.129(4)	2.129(4)	2.136(5)
l(Fe−Cl_t)	0.059(1)	0.059(2)	0.067(3)[g]
κ(Fe−Cl_t) × 10^{-5}	0	0.2(2)[h]	1.9(3)[h]
r_g(Fe−Cl_b)	2.329(5)	2.333(8)	2.350(12)
l(Fe−Cl_b)	0.084(2)	0.084(2)	0.103(9)
κ(Fe−Cl_b) × 10^{-5}	0	2.0(2)[h]	10.9(3)[h]
$\angle_a$(Cl_t−Fe−Cl_t)	124.3(7)	123.5(6)	[123.5][i]
$\angle_a$(Cl_b−Fe−Cl_b)	90.7(4)	90.6(3)	93.5(9)
R(%)[j]	5.0	4.7	4.0

[a] Bond lengths in Å; vibrational amplitudes (l) in Å; bond asymmetry parameters (κ) in $Å^3$; angles ($\angle_a$) in degrees; r_a is the operational parameter in the ED molecular intensity equation, r_g is the thermal average bond length, r_e^M is the estimated experimental equilibrium bond length derived from the thermal average bond length by Morse-type anharmonic corrections; Cl_t refers to terminal and Cl_b to bridging chlorines in the dimer. The geometrical parameters of the present study are weighted averages of the respective parameters of the models in the dynamic analysis. The thermal average r_g parameters of the earlier study[7] were calculated from the published r_a parameters. Error limits are estimated total errors, including systematic errors, and the effects of constraints (the latter only for the high-temperature experiment): $\sigma_t = (2\sigma_{LS}^2 + (cp)^2 + \Delta^2)^{1/2}$, where σ_{LS} is the standard deviation of the least-squares refinement, p is the parameter, c is 0.002 for distances and 0.02 for amplitudes, and Δ is the variation of the parameter upon reasonable changes of the constrained parameters. [b] Thermal average bond angle at the experimental temperature; corresponding to a planar equilibrium structure. [c] Average of the terminal and bridging bond lengths of the dimer in r_a representation. [d] Difference of the terminal and bridging bond lengths in the dimer. [e] Applying our usual procedure for calculating the total errors of this parameter, we get a very small value; therefore, we checked how changing the value of this parameter affected the others. Even very small changes of this parameter, such as a few thousandths of an angstrom, resulted in unacceptable worsening of the goodness-of-fit. It must also be noted that all systematic errors cancel for the differences of bond lengths. Nonetheless, as the total uncertainty of 0.001 Å seems to be unrealistically small, we increased it 3-fold. [f] Difference of the monomer bond length and the terminal bond length of the dimer, constrained at the computed value. [g] Refined together with the corresponding monomer parameter. [h] Refined in group. [i] Constrained at the value determined in the low-temperature experiment. [j] Goodness of fit.

ED Results

Results of the ED analyses are given in Table 3. The experimental thermal average bond length of monomeric $FeCl_3$ from our high-temperature experiment is 2.136(5) Å. Although numerically this value is hardly distinguishable from some of the prior computed r_e values (Table 1), such a coincidence does not mean true agreement because of the different physical meanings of the thermal average and equilibrium bond lengths.[57] In the present work, we estimated the experimental equilibrium bond length by anharmonic vibrational corrections from the r_g parameter; and obtained 2.122(6) Å. The difference of 0.014 Å between our r_g and r_e values is reasonable both in sign and magnitude between these two representations. Note that our computations applied larger basis sets than the ones used previously in the literature.

Results of the reanalysis of the earlier low-temperature experiment can be compared with the original one in Table 3. The two sets of results differ very little because the effect of the stretching anharmonicity at this relatively low temperature is modest. Its effect is more noticeable at the higher temperature as can be seen from the dimer results of the high-temperature analysis; the asymmetry parameter (describing the stretching anharmonicity) is an order of magnitude larger at 900 K than at 460 K.

The geometrical parameters of Fe_2Cl_6 could also be determined from the new experiment, and this made it possible to see the effect of temperature on the thermal average bond lengths. The terminal bond of the dimer lengthens about 0.007 Å, while the bridging bond about 0.017 Å. This is expected, considering the much weaker nature of the bridging bond compared with the terminal one.

It is worthwhile to comment on the rather large difference between the low-temperature experimental value of the terminal bond angle (123.5°) and the calculated one for Fe_2Cl_6 (117°). The refinement always gave an about 124° angle, irrespective of the initial parameters or refinement schemes. Fixing this angle to the computed value gave unacceptably bad agreement. Therefore, we tried to estimate the reliability of this computed value. We optimized the Fe_2Cl_6 structure with constraining the terminal bond angle at 120 and 123.5 degrees, respectively. The energies of these structures differed a mere 0.05 (120°) and 2.6 (123.5)° kJ/mol from the optimized structure with a 117° angle. Apparently, the potential energy does not much depend on the X_t−Fe−X_t angle.

Discussion

The thermal-average bond length of iron trichloride, 2.136(5) Å, was determined from high-temperature gas-phase ED. Its experimental equilibrium bond length, 2.122(6) Å, was also estimated by applying Morse-type anharmonic corrections; agreeing well with the computational result, 2.122 Å; of course, the numerical coincidence is only accidental. This agreement between experiment and computation, together with the similarly good agreement for FeF_3, gives us confidence about the applied methods and basis sets and thus in the computed geometrical parameters of the two heavier iron trihalides, for which experimental bond lengths are not available because of their instability in the gas phase.

The results of the NBO analysis of the monomers are given in Table 4. The 3d orbital occupation of FeF_3 is 5.7e, that is, 0.7e larger than what we would expect for a trivalent iron ion. There is further increase with the size of halogens (6.0, 6.2, and 6.3, for Cl, Br, and I, respectively). The increasing 3d orbital occupation toward the iodide is not surprising as the covalent character of the bond always increases in this direction (see Wiberg bond indices). Nevertheless, the more than six d electrons on iron in the larger trihalides suggests a divalent rather than a trivalent metal. Indeed, the crystals of

(57) Hargittai, M.; Hargittai, I. *Int. J. Quantum Chem.* **1992**, *44*, 1057–1067.

Table 4. NBO Charges, Wiberg Bond Indices, and Natural Electron Configurations of the Metal Atoms at mPW1PW91 Level of Theory

	charges			Wiberg indices		
	Fe	X_t	X_b	Fe−X_t	Fe−X_b	NEC (Fe)[a]
			Monomer, FeX_3			
F	2.048	−0.683		0.34		4s(0.18)3d(5.72)4p(0.03)
Cl	1.472	−0.491		0.52		4s(0.39)3d(6.03)4p(0.05)
Br	1.268	−0.423		0.58		4s(0.47)3d(6.15)4p(0.07)
I	0.977	−0.326		0.64		4s(0.57)3d(6.31)4p(0.09)
			Dimer, Fe_2X_6			
F	2.067	−0.659	−0.750	0.35	0.15	4s(0.19)3d(5.71)4p(0.01)
Cl	1.376	−0.438	−0.501	0.56	0.28	4s(0.43)3d(6.11)4p(0.05)
Br	1.119	−0.356	−0.407	0.62	0.32	4s(0.50)3d(6.24)4p(0.06)
I[b]	0.767	−0.249	−0.269	0.69	0.37	4s(0.59)3d(6.45)4p(0.08)

[a] The 4d NEC is between 0.02−0.05 and 0.02−0.11 for the monomers and dimers, respectively. [b] Fe_2I_6 in C_{2v} point group.

iron tribromide and triiodide lose halogens already at moderate temperatures and decay to dihalides.[8] The strong oxidizing power of the tribromide is also in accord with this observation.

The trend in the dimer molecules is similar, except that the metals have a slightly more ionic nature in Fe_2F_6 than in FeF_3. The other dimers, on the other hand, are more covalent than the corresponding monomers, increasingly so from the chloride toward the iodide. The bridging halogens in the dimer are always more negative than the terminal halogens and this is most pronounced for the fluoride (−0.75e vs −0.66e for the bridging and terminal fluoride, respectively). The enhanced ionic character of the bridging halogens compared with the terminal ones indicates that the dimerization is driven, at least in part, by electrostatic forces and this explains why dimerization is less and less favored as we go toward the triiodides.

The symmetry of the dimer structures is of interest. While the first three trihalides have the expected D_{2h} symmetry, for Fe_2I_6 our computations (see Table 2), both at the DFT and at the MP2 levels, produced a C_{2v}-symmetry, puckered structure. Our earlier calculation of the Al_2I_6 structure gave similar results,[58] although in that case only the MP2 calculations gave puckered structures, while the DFT methods resulted in D_{2h}-symmetry. The DFT calculation of the D_{2h}-symmetry structure of Fe_2I_6 resulted in one imaginary frequency, and the structure lies 4.2 kJ/mol (MP2: 4.1 kJ/mol) higher in energy than the C_{2v} ground-state structure.

We note that the MP2 structure of Fe_2I_6 (Table 2) has peculiar features. The bridging Fe−I bonds are much longer than usual; instead of the 0.2 Å difference compared to the terminal bond, here this difference is over 0.3 Å. Another noteworthy aspect of this structure is the very large terminal bond angle, 159.4° as compared with the DFT value of 115.4°. Both NBO charges and Wiberg indices indicate weak interactions between the atoms; for example, the bond index of Fe−I_b is only 0.15, which is less than half of the DFT value (0.37). It appears as if this method predicts a rather unstable species for Fe_2I_6 that is approximating the dissociation of the molecule into two FeI_2 molecules and two iodine atoms.

The possibility of a low-spin electronic structure for the dimer was examined for iron trichloride. This structure ($^1B_{1g}$) lies about 380 kJ/mol higher in energy than the high-spin state from the Gaussian03 calculation. An MRCI test calculation with MOLPRO predicted an even higher energy difference (625 kJ/mol) between this state and the high-spin ground state. This energy difference is in agreement with the magnetic properties of the crystals, where the magnetic moments are oriented in an opposite way in adjacent layers.[59]

Table 5. Calculated and Experimental Standard Formation Enthalpies (kJ/mol) and Entropies (J/mol·K) for All Iron Trihalide Monomers and Dimers and Sublimation Enthalpies (kJ/mol), Entropies (J/mol.K), and Free Energies (kJ/mol) for Iron Trifluoride and Trichloride at the mPW1PW91 Level[a]

	F		Cl		Br	I
	calc	exp[b]	calc	exp[b]	calc	calc
FeX_3						
$\Delta_f H^0$	−694.6	−820.9	−249.7	−253.1	−139.0	−22.3
S^0	312.6	304.1	344.8	344.2	380.2	405.9
$\Delta_{sub}H^0$	347.2		146.4			
$\Delta_{sub}S^0$	214.3		202.6			
$\Delta_{sub}G^0$	283.3		85.9			
Fe_2X_6						
$\Delta_f H^0$	−1561.6		−650.3	−654.4	−311.5	−155.5
S^0	463.3		528.8	536.9	608.5	668.0
$\Delta_{sub}H^0$	522.0		141.7			
$\Delta_{sub}S^0$	266.7		244.4			
$\Delta_{sub}G^0$	442.5		68.9			

[a] The atomic data of ref 62 were used for the calculation. Crystal formation enthalpy (FeF_3: −1041.8 and) and entropies (FeF_3: 98.3 and $FeCl_3$: 142.2 J/mol.K) are from ref 60, and formation enthalpy of $FeCl_3$ (−396.0 kJ/mol) is from ref 61. [b] Ref 60.

Thermodynamic data for the monomers and dimers were also calculated. Table 5 shows the standard formation enthalpies of all iron trihalides, together with the available (only for FeF_3, $FeCl_3$, and Fe_2Cl_6) experimental data from the JANAF tables.[60] For iron trichloride the agreement is good, while there is a large (126.2 kJ/mol) difference for FeF_3. The decreasing enthalpy of formation toward the iodides corresponds to the decreasing stability of these halides in the series.

The enthalpy of sublimation can be calculated as the difference of the enthalpies of formation of the gas-phase iron trichloride dimer and the iron trichloride crystal,[61] these are also given in Table 5. While the enthalpy of sublimation for the monomer $FeCl_3$, 146.4 kJ/mol, is only slightly higher than that for the dimer, 141.7 kJ/mol, the free energies of sublimation ($FeCl_3$: 85.9 and Fe_2Cl_6: 68.9 kJ/mol) already suggest larger vapor pressure for the dimer, indicating that this is mostly an entropy effect. For iron trifluoride, both the sublimation enthalpies and the free energies favor the monomer.

We also calculated the structure of other small oligomers of $FeCl_3$, to see whether a connection with the crystal structure emerges or not. For the trimer, three isomers, shown in Figure 3, were calculated. The ground state structure has two four-member rings connected, and the ninth chlorine is bonded to the central iron atom. The other two structures are much higher in energy; with the third one being only a transition state. In contrast, for the tetramer, the three lowest-energy structures, all consisting of connected four-member

(58) Hargittai, M.; Reffy, B.; Kolonits, M. *J. Phys. Chem. A* **2006**, *110*, 3770–3777.

(59) Cable, J. W.; Wilkinson, M. K.; Wollan, E. O.; Koehler, W. C. *Phys. Rev.* **1962**, *83*, 35–41.

(60) Chase, M. W., Jr. *NIST-JANAF Thermochemical Tables*, 4th ed.; American Chemical Society: Washington, DC, **1998**.

(61) Blairs, S. *J. Chem. Thermodyn.* **2006**, *38*, 1484–1488.

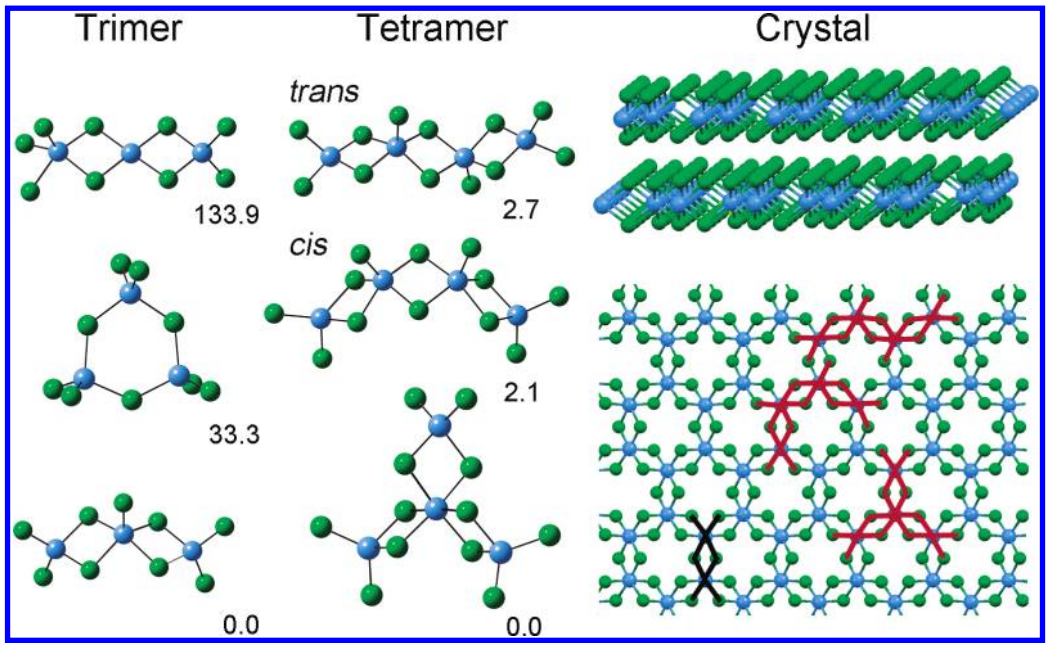

Figure 3. Molecular structure of iron trichloride trimers and tetramers (with their relative energies in kJ/mol), and the crystal structure in two representations. Some tetramers and a dimer in the crystal structure are highlighted to indicate their relationship to the crystal structure.

rings, are very close in energy, as shown in Figure 3. In the ground-state structure of the tetramer, the fourth monomer unit attaches to the central iron atom of a trimer, thus providing six-coordination to the central metal atom. The other two low-energy excited-state molecules have a chain structure.

Comparison of the structures of the same substance in different phases may be instructive in learning about intermolecular and interionic interactions.[63] For metal halides, because of the ionic nature of the crystals and the different coordination numbers of the metals in different phases, the structure of the free molecule is usually too different from the crystal to find any obvious correlation. If the structural unit of a gas-phase species, for example, a dimer, can be "recognized" in the crystal, the chance of finding these species in the vapor is enhanced.[63,64] This happens in iron trichloride, whose crystals consist of octahedra sharing edges (Figure 3). For iron trifluoride, its crystal consists of octahedra sharing vertices; its vapors do not contain dimers.

The dimer of iron trichloride seems to be a very stable unit; from the melt to relatively high temperature gases (it is even present in the hot gas at 900 K). It can also be "recognized" in the crystal as highlighted in Figure 3. Figure 3 illustrates that all three low-energy tetramers can be "recognized" in the crystal structure, so they might be candidates for the first steps toward crystallization. In this respect, although the ground-state tetramer structure shows six-coordination around iron, it is not a good candidate for crystallization; this structure cannot be formed easily from two dimers. For this, the slightly higher-energy cis or trans structures are better candidates. Of course, the process of crystallization is a complex matter, but the fact that the dimers and tetramers are "recognizable" in the crystal suggests that there may be no need for extensive rearrangement.

Acknowledgment. We acknowledge the support of the Hungarian Scientific Research Fund (OTKA K 60365) and the additional computer time of the National Information Infrastructure Development Program of Hungary.

Supporting Information Available: Cartesian coordinates of isomers of iron trichloride trimers and tetramers (Table S1); computed vibrational frequencies, together with experimental ones from the literature for all iron trihalide monomers (Table S2) and dimers (Table S3); computed free energies of dimerization for the experimental temperatures (Table S4); experimental ED molecular intensities at two different camera ranges for the high-temperature experiment of iron trichloride (Table S5), and the extent of dimer contribution to the molecular intensities (Figure S1). This material is available free of charge via the Internet at http://pubs.acs.org.

(62) Burcat, A.; Ruscic, B. *Third Millennium Ideal Gas and Condensed Phase Thermochemical Database for Combustion with Updates from Active Thermochemical Tables*; Argonne National Laboratory: Argonne, Illinois, 2005.
(63) Hargittai, M.; Hargittai, I. *Phys. Chem. Miner.* **1987**, *14*, 413–425.
(64) Hargittai, M.; Jancso, G. *Z. Naturforsch., A: Phys. Sci.* **1993**, *48*, 1000–1004.